

Petrologic History of Moon Suggested by Petrography, Mineralogy, and Crystallography

Abstract. Opaque mineral compositions indicate that the fugacity of oxygen is approximately 10^{-13} (earth basalts, 10^{-10}). Experiments under reducing conditions suggest that the crystallization range is approximately 1140° to 1070°C . Iron-rich pyroxmangite, fayalite, and hedenbergite occur in microgabbro. Ferropseudobrookite rimmed by ilmenite containing rutile and Cr-spinel lamellae occurs in ferrobasalt. Plagioclase vitrophyres in breccia can explain highland Surveyor VII analysis. We suggest crystal-liquid differentiation of out-gassed convecting moon with growing Fe-rich core, olivine-pyroxene mantle, plagioclase-rich dynamic crust underlain by nonspherical, inversely stratified ferrobasalt. Impact-breaking or convection-thrusting of crust releases fraction rich in Fe and Ti. Scanning electron microscopy of glass balls reveals minute depressions consistent with micrometeorite impact.

Type A ferrobasalts 22, 57, and 72, type B microgabbros 44 and 47, type C breccia 61, and type D 84 and 85 soil (1) yielded optical and electron microscope data, x-ray diffraction patterns, and electron microprobe analyses. We concentrated on evidence of crystal-liquid differentiation, particularly in the breccia which contains plagioclase- and olivine-vitrophyres as well as fragments of ferrobasalts.

Petrography and mineralogy of basalts and microgabbros. Ferrobasalts are vesicular containing sporadic olivine and ferropseudobrookite phenocrysts within fine-grained augite with intergrown pigeonite, ilmenite, plagioclase, and devitrified, microvesicular residual glass. Microgabbros lack phenocrysts and contain coarse-grained augite (strongly

zoned), Fe-rich pyroxmangite, ilmenite, plagioclase, low-cristobalite, and a symplectitic residuum of fayalite and hedenbergite composition. Ferrobasalt fragments in breccia contain more residual glass than individual ferrobasalts, while some are entirely devitrified glass without microphenocrysts,

Ferrobasalts and microgabbros petrographically and chemically resemble coarse segregation veins or schlieren in terrestrial basalts formed from Fe-Ti-rich residual liquid flowing into cracks and crystallizing (2, 3). Figure 1 shows compositions of selected minerals and glasses.

Ilmenite in ferrobasalt occurs as rims to ferropseudobrookite phenocrysts (Gi 13), early crystals lining vesicles (Gi 11), later tabular crystals (Gi 6) in areas rich

in ilmenite and pyroxene, and finally as plates (Gi 3 to 0.3) restricted to plagioclase-glass rich regions [Gi, mole percent MgTiO_3]. The very low Fe_2O_3 content increases slightly with crystallization. Ilmenite in microgabbro ranges from center of large crystal (Gi 3; Cr_2O_3 , 0.7; MnO , 0.3 weight percent) to tiny crystal associated with residuum fayalite (Gi 0.4; Cr_2O_3 , 0.05; MnO , 0.6 weight percent).

Ferropseudobrookite (FeTi_2O_5) megacrysts in ferrobasalts 22 and 72 and ferrobasalt fragments in breccia 61 are rimmed invariably by ilmenite containing lamellae of rutile and Cr-rich spinel.

Ulvospinel occurs in the residuum of microgabbro 44.

Troilite ($\text{Fe}_{1.02}\text{Cu}_{0.00}\text{Ni}_{0.00}\text{S}$) occurs as subspherical interstitial grains in basalt and microgabbro enclosing tiny metallic iron particles ($\text{Fe}_{0.97}\text{Ni}_{0.003}$) yielding bulk composition of approximately $\text{Fe}_{1.1}\text{S}$. The complex texture of some iron suggests unmixed oxide, carbide, or phosphide, or all three. The invariable troilite-iron assemblage suggests an Fe-S liquid immiscible with the silicate.

Subcalcic augite is predominant in both ferrobasalt and microgabbro. Except for lower Ca, the zoning (Fig. 1A) parallels that of terrestrial basaltic pyroxenes (4) and ranges from hour-glass to irrational planar sector zoning. The subcalcic augite of ferrobasalt has a smaller composition range than for the microgabbro, and is further distinguished by containing small patches of pigeonite. The microgabbro pyroxene (Fig. 1A) zones discontinuously into almost Mg-free metasilicate, which may be iron-rich pyroxmangite.

Subcalcic augites in ferrobasalt contain (weight percent) 6 to 1.5 Al_2O_3 , 4.1 to 1.1 TiO_2 , 0.15 to 0.26 MnO (no data for Fe-rich specimens), and 0.6 to 0.1 Cr_2O_3 (no data for Fe-rich specimens) as compared with 2 to 0.6 Al_2O_3 , 1.7 to 0.9 TiO_2 , 0.3 to 0.7 MnO , and 0.3 to 0.1 Cr_2O_3 in microgabbro.

Pyroxmangite is the unidentified yellow mineral of the microgabbro (1). Single crystals from sample 44 yielded: triclinic a 6.61, b 7.54, c 17.3 Å; α 114.3° , β 82.7° , γ 94.6° (Table 1, analysis A). With stereomicroscopy, yellow pyroxmangite clearly abuts cinnamon pyroxene; in thin section, distinction is difficult. On earth, pyroxmangite has $\text{Fe}/(\text{Fe} + \text{Mn})$ ratio below 0.6; however terrestrial Fe-rich pyroxmangite might have been confused with pyroxene.

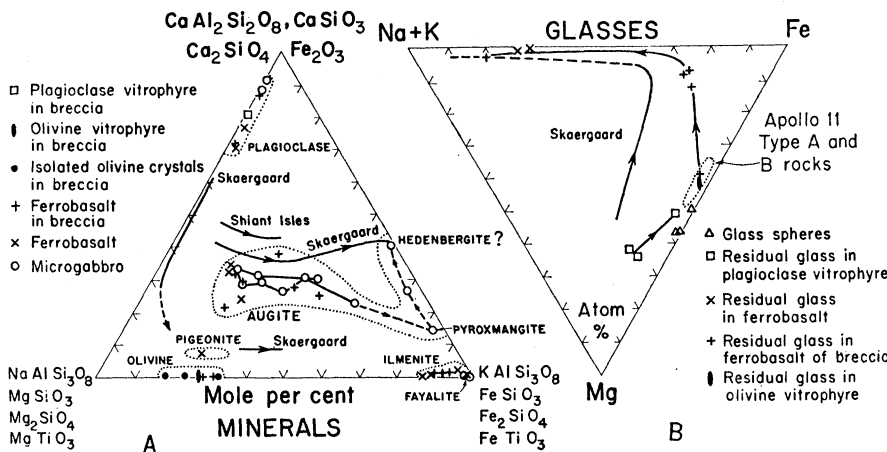


Fig. 1. (A) Compositions of minerals from Apollo 11 rocks. End members and minor element data which apply to different minerals are: plagioclase [$\text{CaAl}_2\text{Si}_2\text{O}_8$, $\text{NaAlSi}_3\text{O}_8$, and KAlSi_3O_8 (mole percent)], pyroxenes and pyroxmangite (CaSiO_3 , MgSiO_3 , FeSiO_3 , 0.15 to 0.7 MnO , 0.3 to 0.1 Cr_2O_3 , 8 to 1 Al_2O_3 , 4 to 1 TiO_2 , data for augites only; Al and Ti are highest in augites from ferrobasalts), olivine (Ca_2SiO_4 , Mg_2SiO_4 , Fe_2SiO_4 , 0.00 to 0.03 Ni, 0.14 to 0.29 Mn, 0.8 Mn in fayalite), ilmenite (Fe_2O_3 , MgTiO_3 , FeTiO_3 , 0.5 to 0.0 Al_2O_3 , 0.8 to 0.3 Cr_2O_3 , 0.4 to 0.9 MnO). Comparison curves for Shiant Isles and Skaergaard pyroxenes and plagioclases from (4, 8). (B) Iron, magnesium, and alkali diagram of glasses from Apollo 11 rocks. Arrows on lines of liquid variation point toward increasing solidification. Comparison curve for estimated Skaergaard liquids from (8). For relations of plagioclase vitrophyre and ferrobasalt see petrogenesis section. Composition of glass beads indicates volatile loss of Na and K.

Table 1. Microprobe analyses mentioned in text (weight percent). The analyses are: A, pyroxmangite, rock 10044; B and D, devitrified glasses in fragments of ferrobasalt in breccia 10061; C, devitrified glass in ferrobasalt 10022; E, devitrified glass (90 percent) in plagioclase vitrophyre in breccia 10061; F, glass (70 percent) in olivine vitrophyre in breccia 10061; and G, synthetic glass used for melting experiments.

Oxide	Analysis						
	A	B	C	D	E	F	G*
SiO ₂	45.6	56	62	73	46	54	43
TiO ₂	0.3	2	0.35	1.2	0.6	1.0	10
Al ₂ O ₃	1.1	19	23	13	24	17	10
FeO	45.9	14	3	2.4	5	10	19
MnO	0.6	0.3		0.2			0.4
MgO	0.6	1	0.1	0.2	0.7	4	6.5
CaO	5.9	8	9	2.1	15	14	9.7
Na ₂ O	0	1.4	1.7	0.5	1	0.1	0.5
K ₂ O	0	0.9	2.3	5.5	0.06	0.02	0.16
P ₂ O ₅	0	0.3	0.09	0.3	0.02	0.02	

*Also Cr₂O₃ 0.47 and ZrO₂ 0.16.

Olivines (69 to 72 mole percent Mg₂SiO₄) from two ferrobasalt fragments in breccia 61 have (Fo₆₉₋₇₂), Mn 0.25, Ca 0.19, and Ni 0.00 to 0.01 (weight percent). The Mn and Ca contents fall in the range of terrestrial volcanic olivines, but the Ni content is less (5).

Plagioclase in ferrobasalt grows into hollow, square tubes (extreme hopper structure) which enclose devitrified liquid and other phases. Bytownite up to An₈₇Or_{1.5} is typical, but adjacent to rhyolitic residual glass An₇₁Or₂ occurs.

Devitrified glass in ferrobasalts varies in quantity and composition from that of ferrobasalt itself to "andesite", to "anorthosite", and to "rhyolite" (Table 1, analyses B, C, and D).

Symplectic residuum in microgabbros

consists of fayalite and metasilicate of composition near hedenbergite (Fig. 1A).

Low-cristobalite which is spatially associated with the residuum of the microgabbro and the rhyolitic composition of residual glass in ferrobasalt emphasize the silica saturation of Apollo 11 rocks evident in their norms (~10 percent SiO₂).

Although the vesicularity of ferrobasalts indicates past presence of gases, none of the rocks shows obvious evidence of alteration.

Breccia contains ferrobasalt and minerals at various states of shock including melting (i) glass beads—clear to red brown; (weight percent) SiO₂ 35 to 42, TiO₂ 0.6 to 10, Na₂O <0.1, and K₂O

<0.02; glassy to spherulitic; some bubbles; rare crystal ghosts and small blebs of Fe metal; (ii) irregular fragments of vesicular glass—clear to yellow, brown, or green; glassy to devitrified; many vesicles; anhedral crystal relics; blebs of Fe (<4 percent Ni) surrounded by halos of Fe-poor glass; rare microlites; (iii) glass rims on rock fragments—clear to yellow-brown; similar to (ii) but fewer Fe blebs and more devitrified; origin; melting by external heating possibly involving hot, impact-generated gas; (iv) plagioclase vitrophyres—clear, almost nonvesicular, euhedral or dendritic plagioclase microphenocrysts; metal absent; composition (Table 1, analysis E); (v) olivine vitrophyres—pale-brown, nonvesicular, skeletal olivine; no metal; composition of 70 percent residual glass (Table 1, analysis F).

Soil has similar constituents to breccia, showing similar x-ray and microprobe data for minerals. Fragments of meteoritic iron are rare.

Glass balls show complex surface features under hard-vacuum, scanning electron microscopy—for example (i) minute, rubble-filled, circular, lipped depressions consistent with micrometeorite impact (Fig. 2), (ii) dimpled (golf-ball) surface, and (iii) deformed surface with small angular fragments sticking to surface. The phenomena are consistent with spheres of varying rigidity and stickiness falling onto soil. Surface tension shaping of fiery rain and collision deformation and breakage ex-

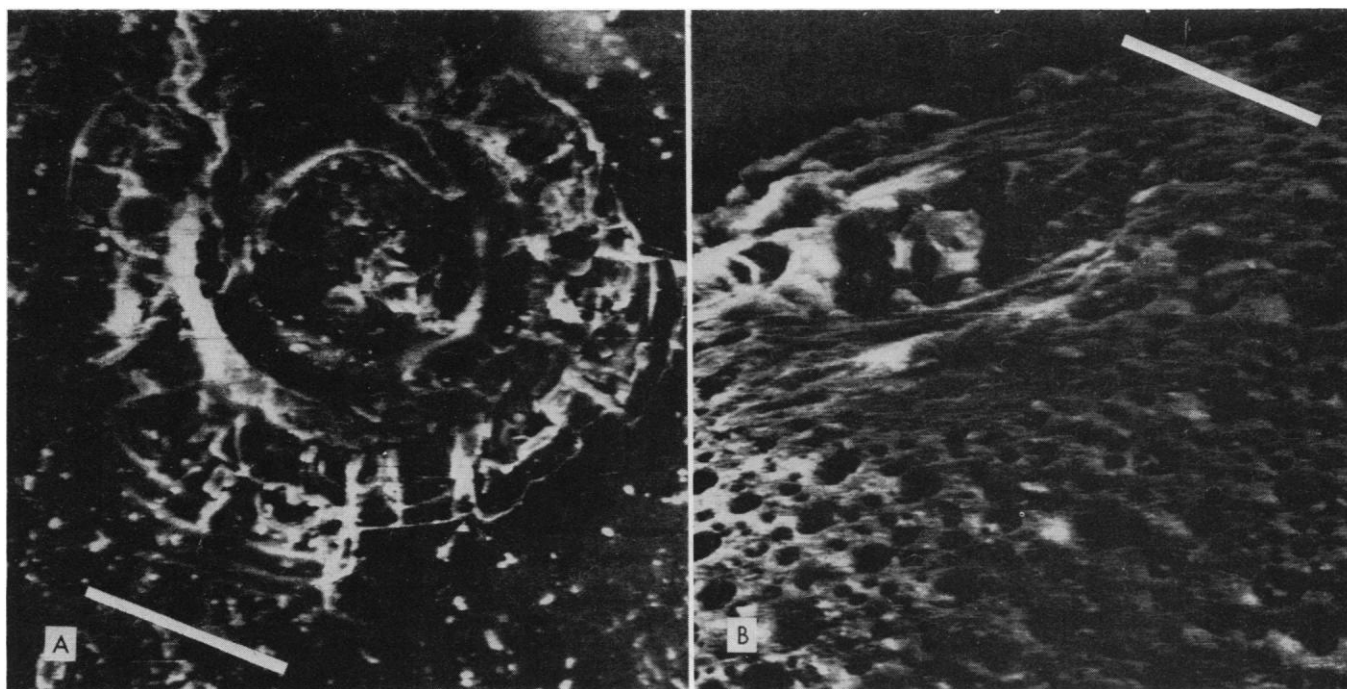


Fig. 2. Scanning electron micrographs of surfaces of glass balls. (A) Impact crater, scale 24 μm ; (B) dimples, scale 14 μm .

plain many features. Some balls contain cavities.

Melting experiments. Synthetic ferrobasalt glass (Table 1, composition G) was heated in stoppered iron capsules in evacuated silica tubes from 1½ to 12½ hours and then water-quenched. The results showed that at 1235°, 1185°, and 1155°C, it was all glass; at 1125°C, 70 percent glass, the rest being ilmenite and pyroxene; at 1100°C, 30 percent glass, the rest being ilmenite, pyroxene, plagioclase; and at 1075°C, <10 percent glass. Small Fe metal beads pervade the glass. Ilmenite has <1 percent Fe₂O₃. The low liquidus temperature (~1140°C) and narrow melting range are similar to those in basaltic segregation veins (3) and are suggestive of a differentiation origin of ferrobasalt. The mineral sequence agrees with textural interpretation of Apollo 11 ferrobasalts.

Petrogenesis. Outgassing of the moon probably was more extensive than that of the earth because of the lack of visible alteration and low Na₂O content of Apollo 11 ferrobasalt and microgabbro. Although the more calcic nature of Apollo 11 than terrestrial basaltic plagioclase might result from incorporation of Al in high-pressure phases of the earth's mantle not found on the moon, the sodic nature of chondritic plagioclase suggests volatile loss of Na from the moon as evidenced by the extremely low Na₂O and K₂O contents of the glass beads. The extreme zoning of pyroxenes may result from a paucity of catalyzing volatiles.

Reduction of the moon was greater than that of the earth but similar to ordinary chondrites (6) since the oxygen fugacity of the ferrobasalts and microgabbros, as estimated from compositions of iron silicate, oxide, sulfide, and metal phases with the use of standard thermochemical data, is about 10⁻¹³ at 1100°C compared to 10⁻¹⁰ for earth basalts (7). The following data support a greater reduction of the moon: Low Ni in olivine (greater reduction to metal) and low P₂O₅/K₂O ratio (greater solution of P in metal).

Differentiation of the moon occurred of a type similar to that of the earth except for differences due to the moon's extreme reduction and volatile outgassing as well as smaller mass. Variation in liquid composition with crystallization of ferrobasalt is similar to that of the Skaergaard intrusion (8) except for lower alkalis (Fig. 1B). In ferrobasalt, a sulfide melt, ilmenite and

augite separate early from silicate melt and are joined by plagioclase only after semisolidification as evidenced by fragments in breccia of glassy ferrobasalt containing only euhedral ilmenite and pyroxene, blebs of sulfide and devitrified glass.

Plagioclase vitrophyres (in breccia) contain 70 percent normative plagioclase and probably are fragments of highland material because their composition is close to that of Surveyor VII (9). Because they have much more soda than glass beads (which are almost certainly impact fused ferrobasalts, microgabbros and their minerals) and lack blebs of Fe metal, the plagioclase vitrophyre fragments probably were not superheated on a small (grain size) scale. Crystallization of plagioclase vitrophyres produces glasses which trend toward ferrobasalt composition on an alkali, iron, magnesium (AFM) diagram (Fig. 1B) but which have less TiO₂ and more Na₂O.

The ferrobasalts and plagioclase vitrophyres are complementary: the delayed appearance of plagioclase in ferrobasalts (density, 3.54 g/cm³) corresponds to the super-abundance of plagioclase in the plagioclase vitrophyres (density, 3.0 g/cm³). The TiO₂/K₂O ratio ranges from 6.7 to 10 in three plagioclase vitrophyres but is 28 in ferrobasalt suggesting either addition of Ti to or loss of K from ferrobasalt. Tentatively we explain these facts by gravitative separation of plagioclase (2.8 g/cm³), augite (3.4 g/cm³), ilmenite (4.7 g/cm³), and liquid (3.1 g/cm³) followed by melting of liquid plus plagioclase mush and liquid plus augite plus ilmenite mush yielding plagioclase vitrophyre and ferrobasalt liquids respectively.

Breccia cohesiveness (1) may result from thermal sintering from hot gas and ash clouds. Impact rather than volcanic origin of the cloud is indicated since vesicular, glassy rims require high superheating. Thermal sintering is favored over impact compaction because of preservation of thin-walled vacuoles in some spherules.

Proposed petrologic history of the moon. Our data and petrogenetic interpretations suggest, in the light of previous studies (10), the following model for the evolution of the moon. (a) Initially the moon was melted sufficiently for Mg-rich olivine and pyroxene to settle towards the center, perhaps around an iron-rich core. Major chemical fractionation took place by crystallization

within the interior and by loss of volatiles from the surface. (b) Iron content and density of the convecting liquid mantle of the moon increased as successive shells were formed. Convection-thrusting and impact-breaking continually disrupted a thin primitive crust rich in olivine and pyroxene. (c) After about 80 percent of the initial mass had crystallized (to within about 130 km of the surface), plagioclase commenced to form and the iron and titanium content and density of the remaining liquid rapidly increased. Plagioclase flotation created the first substantial crust—now the lunar highlands. (d) Gravitational pull of some body in the solar system caused concentration of the dense liquid on the present nearside of the moon and antipodal bulge of light crust on the farside. (e) Ilmenite crystallized and sank, forming TiO₂-rich cumulates at the base of the liquid layer, which now amounted to <5 percent of the lunar mass. (f) Impacting bodies (11) continued to destroy the thin nearside crust exposing large areas (seas) of ferrobasalt liquid and creating additional liquid by impact melting of cumulates. Impacting bodies of the same energy would form only large, deep craters on the thick farside crust. (g) After total solidification, local remelting possibly caused explosive volatilization and ash flow emplacement of breccia deposits.

Several tests of this model are possible. (i) The proposed density stratification, especially the inverse stratification, could be tested for by a large seismic array. (ii) A search could be made for cumulate rocks and primitive olivine-pyroxene crust. (iii) A higher heat flow on the nearside would follow from concentration of radioactive elements in the residual liquid.

A. T. ANDERSON, JR.

*Department of the Geophysical Sciences,
University of Chicago,
Chicago, Illinois 60637*

A. V. CREWE

*Department of Physics,
Enrico Fermi Institute, Chicago*

J. R. GOLDSMITH

P. B. MOORE, J. C. NEWTON
*Department of the Geophysical Sciences,
University of Chicago*

E. J. OLSEN

*Department of the Geophysical Sciences
and Field Museum of Natural History,
University of Chicago*

J. V. SMITH

P. J. WYLLIE
*Department of the Geophysical Sciences,
University of Chicago*

References and Notes

1. Lunar Sample Preliminary Examination Team, *Science* **165**, 1211 (1969).
2. H. Kuno, *J. Petrol.* **6**, 302 (1965).
3. C. E. Tilley, H. S. Yoder, Jr., J. F. Schairer, *Carnegie Inst. Wash. Yearbook* **62**, 77 (1963).
4. G. M. Brown, *Mineral. Mag.* **31**, 511 (1957); R. J. Murray, *Geol. Mag.* **91**, 17 (1954).
5. T. Simkin and J. V. Smith, *J. Geol.*, in press.
6. R. F. Mueller, *Geochim. Cosmochim. Acta* **28**, 189 (1964).
7. R. F. Fudali, *ibid.* **29**, 1063 (1965); I. S. E. Carmichael and J. Nicholls, *J. Geophys. Res.* **72**, 4665 (1967); A. T. Anderson, Jr., *Amer. J. Sci.* **266**, 704 (1968).
8. L. R. Wager and W. A. Deer, *Medd. Grönland* **106**, 1 (1939); L. R. Wager, *J. Petrol.* **1**, 364 (1960).
9. A. L. Turkevich, E. J. Franzgrote, J. H. Patterson, *Science* **162**, 117 (1968).
10. P. D. Lowman, Jr., *J. Geophys. Res.* **74**, 495 (1969); R. T. Reynolds and A. L. Summers, *ibid.*, p. 2495; Y. Nakamura and G. V. Latham, *ibid.*, p. 3771.
11. G. P. Kuiper, *Proc. Nat. Acad. Sci. U. S. A.* **40**, 1096 (1954).
12. We thank M. Isaacson and D. Johnson for electron microscopy, R. Zechman and O. Draughn for microprobe operation, G. A. Desborough for sulfide standards, the Clayton and Hafner groups for sample cooperation, and R. Banovich, A. Devitt, and I. Baltuska for technical help. We thank J. Warner of NASA for excellent cooperation. Supported by NASA grant NAS 9-8086. We thank NSF (grants G-1658, GA-4420, and GA-1656), ARPA, Union Carbide Corporation, Herz Foundation, and University of Chicago for basic and specific support.

4 January 1970

Electron Microprobe Analysis of Lunar Samples

Abstract. *Plagioclase feldspar, clinopyroxene, and ilmenite in a polished thin section of a type A crystalline rock were analyzed. The clinopyroxene grains are compositionally variable, and both high Ca and low Ca phases are present. The plagioclase is compositionally homogeneous. The ilmenite is chemically homogeneous except for occasional, small areas of high local chromium concentration. Accessory minerals are: apatite (containing Cl, F, Y, and Ce), troilite, and metallic iron. Glassy spherules from the lunar soil are for the most part similar in composition to the crystalline rocks; however, some appear to have been monomineralic. The crystalline rock has apparently formed by relatively rapid cooling of a silicate melt under conditions of low oxygen partial pressure. Many components of the soil appear to have formed by meteoritic impact.*

We present here electron microprobe and petrographic analysis of Apollo 11 samples of a crystalline rock and separates from a soil sample. A polished thin section of sample 10017-16 was examined microscopically. The sample is an equigranular, crystalline rock in which most crystals are about 0.5 to 1.0 mm in largest dimension. In transmitted light, four major phases can be recognized: (i) clinopyroxene, which occurs as short subhedral crystals; (ii) plagioclase, occurring as anhedral lath-shaped crystals; (iii) opaque minerals, dominantly euhedral ilmenite; and (iv) a partly crystalline, very fine-grained intergranular mesostasis containing several phases. A few vesicles, generally

circular and about 1 mm in diameter, constitute about 5 percent by volume of the sample.

The modal mineral composition of the sample, determined by point counting (816 points, 200 mm² area), was (in percent by volume): clinopyroxene, 49.7; plagioclase, 18.0; opaque minerals, 23.9; and mesostasis, 8.3. The subophitic texture of the sample and the modal mineral composition are typical of the type A crystalline rocks described by the Preliminary Examination Team (PET) (1).

The clinopyroxene is colorless to very pale reddish-brown. The crystals do not exhibit definite pleochroism or color-zoning, and no reaction rims were ob-

served at the contacts with other minerals. There is an irregular cleavage in the clinopyroxene grains. The extinction angle $Z \wedge c$ is about 45°, thus indicating an augite. The plagioclase is apparently unzoned. The pyroxene grains are slightly fractured, but neither pyroxene nor plagioclase shows any evidence of shock metamorphism. Distinctive shock features such as intense fracturing, "planar features," or isotropization of plagioclase were not observed. In view of this lack of evidence for shock metamorphism of the major minerals, it seems clear that the mesostasis cannot be shock-melted glass and that it probably represents residual crystallization of the melt from which the sample formed.

Although sample 10017-16 does not contain olivine, it has a mineral composition consistent with the chemistry of other samples (1) and is representative of the material at the Apollo 11 landing site.

The plagioclase phase of sample 10017-16 appears generally homogeneous both between grains and within individual grains. The average composition of the plagioclase is SiO₂, 49 percent; CaO, 16 percent Al₂O₃, 33 percent; total iron as FeO, 1 percent; TiO₂, 0.2 percent; K₂O, 0.2 percent; Na₂O, 2 percent; and anorthite, 76 percent.

In contrast, the clinopyroxenes in the sample appear heterogeneous both between grains and within grains. Most of the measured compositions center around 30 atom percent FeSiO₃, 30 atom percent CaSiO₃, and 40 atom percent MgSiO₃. Some pyroxene crystals show bands and regions of higher atomic number due to higher iron concentrations (see Fig. 1). These areas appear to be a second pyroxene phase with low calcium concentration (pigeonite?) at the boundaries of the prevalent pyroxene phase (Table 1).

Table 1. Representative composition of various phases in crystalline rock 10017 (type A).

Sample	Weight percentages as oxide									Sum
	Na	Mg	K	Al	Si	Ca	Ti	Mn	Fe as FeO	
Pyroxene		14.6		3.3	49.6	15.8	2.3		15.1	100.7
Pyroxene		15.9		3.6	49.6	17.0	2.7		9.9	98.7
Pyroxene		12.4		2.2	49.4	14.0	1.7		19.5	99.4
Pyroxene		20.8		0.9	52.0	4.1	0.8		21.5	100.2
Ilmenite		0.91		0.63	0.11		52.8	0.34	46.1	100.9
Ilmenite		0.88		0.71	0.12		51.4	0.33	46.5	100.0
Spherule (130-3)	0.2	5.0	0.1	12.5	42	14	7.4	0.18	16.5	98.4
Spherule (L-8)	0.3	11	0.1	13	46	12	2.5	0.14	15	100
Spherule (122)	0.5	13	0.16	4.5	37	8	10	0.24	24.5	97.9
Spherule (128)	3.0	13.5	0.06	7.4	43	10	0.5	0.19	21.2	96.2
Spherule (129)	0.7	5.4	0.1	24.5	47	16	0.5	0.07	5.7	100